

# Studies on the influence factors of wind dynamic responses on hyperbolic cooling tower shells

Jun-Feng ZHANG<sup>\*1</sup>, Qing-Shuai LIU<sup>1</sup>, Yao-Jun GE<sup>2a</sup> and Lin ZHAO<sup>2b</sup>

<sup>1</sup>School of Civil Engineering, Zhengzhou University, Zhengzhou 450001, China

<sup>2</sup>State Key Laboratory for Disaster Reduction in Civil Engineering, Tongji University, Shanghai 200092, China

(Received December 29, 2018, Revised March 20, 2019, Accepted March 21, 2019)

**Abstract.** Wind induced dynamic responses on hyperbolic cooling tower (HCT) shells are complicated functions of structure and wind properties, such as the fundamental frequency  $f_{\min}$ , damping ratio  $\zeta$ , wind velocity  $V$ , correlation in meridian direction and so on, but comprehensions on the sensitivities of the dynamic responses to these four factors are still limited and disagree from each other. Following the dynamic calculation in time domain, features of dynamic effects were elaborated, focusing on the background and resonant components  $\sigma_B$  and  $\sigma_R$ , and their contributions to the total rms value  $\sigma_T$ . The  $\sigma_R$  is always less than  $\sigma_B$  when only the maximum  $\sigma_T$  along latitude is concerned and the contribution of  $\sigma_R$  to  $\sigma_T$  varies with responses and locations, but the  $\sigma_R$  couldn't be neglected for structural design. Then, parameters of the above four factors were artificially adjusted respectively and their influences on the gust responses were illustrated. The relationships of  $\sigma_R$  and the former three factors were expressed by fitted equations which shows certain differences from the existing equations. Moreover, a new strategy for wind tunnel tests aiming at surface pressures and the following dynamic calculations, which demands less experiment equipment, was proposed according to the influence from meridian correlation.

**Keywords:** hyperbolic cooling towers; wind induced dynamic responses; background component; resonance component; gust response factor; fundamental frequency; damping ratio; wind velocity; meridian correlation

## 1. Introduction

Studies on the wind dynamic effects on hyperbolic cooling towers (HCTs) have last for more than fifty years because wind loading plays a significant role in the structural design of HCTs and the gust properties and dynamic effects are inherent characteristics of wind. Based on some wind tunnel tests and calculations, the dynamic effects are always expressed by equivalent static wind loads (ESWLs) in structure design codes, such as BS 4485, VGB-R 610Ue and GB/T 50102. It's well known that wind dynamic effects on structures are functions of properties of structure and wind: the former includes the frequencies, mode shapes and structural damping ratio, the latter includes the velocity, turbulence intensity, velocity spectrum and spatial correlation. However, when a study is conducted taking a certain HCT under specific wind loading as an example (Davenport and Isyumov, 1967, Isyumov *et al.* 1972, Abu-Sitta and Hashish, 1973, Steinmetz *et al.* 1978, Niemann and Ruhwedel, 1980, Basu and Gould, 1980, Sollenberger *et al.* 1980, Kapania and Yang, 1984, Kasperski and Niemann, 1988, Chen and Wei,

2003, Zhao *et al.* 2008, Ke *et al.* 2012, Zou *et al.* 2013, Zhang *et al.* 2017), there is no way to understand the influences of these parameters. Moreover, the understanding on these parameters would be further confused when the interference effects are incorporated, although the interference effects are always hotspots for wind effects on HCTs (Ke *et al.* 2018a, Ke *et al.* 2018b, Zhao *et al.* 2018). It's evident that the influences of these factors on the wind dynamic effects should be comprehensively understood for safe and economic structural design. Demand for the influence mechanism is further increased by the planning and construction of increasingly tall and relatively thinner HCTs for future need, especially in developing countries (Babu *et al.* 2013, Zhao *et al.* 2014).

Actually, this question is always under consideration. Wind velocity maybe the easiest factor could be studied by experiments (Armitt, 1973, Armitt, 1980) or calculations (Hashish and Abu-Sitta, 1974, Niemann, 1980). Then, the resonant response component  $\sigma_R$  was always expressed as the function of a dimensionless parameter  $V/f_{\min}D_T$  (Eq. (1)~ Eq.(3)) (Hashish and Abu-Sitta, 1974, Armitt, 1980, Niemann, 1980, Lu *et al.* 1982, Niemann, 1984), which is called reduced velocity. It means the influences of the other two parameters  $f_{\min}$  and  $D_T$  could be deduced by the reduced velocity. As a basic parameter in wind engineering, its rationality and validation for the application has never been discussed yet. Moreover, the relationships of  $\sigma_R$  and  $V/f_{\min}D_T$  got from different studies exhibit quite difference (Eq.(1) ~ Eq.(3)), although Eq.(2) and Eq.(3) are adopted by codes BS 4485 and VGB-R 610Ue correspondingly.

\*Corresponding author, Associate Professor

E-mail: [brilliantshine@163.com](mailto:brilliantshine@163.com)

<sup>a</sup> Professor

E-mail: [yaojunge@tongji.edu.cn](mailto:yaojunge@tongji.edu.cn)

<sup>b</sup> Professor

E-mail: [zhaolin@tongji.edu.cn](mailto:zhaolin@tongji.edu.cn)

$$\sigma_R = K_1 \left( \frac{V_G}{f_{\min} D_T} \right)^{3.4-3.75} \quad (1)$$

by Hashish and Abu-Sitta (1974)

$$\sigma_R = K_2 G \frac{V^4}{f_{\min}^2} \quad (2)$$

by Armit (1980)

$$\sigma_R^2 = K(\zeta) \left( \frac{D_T}{L} \right)^{2/3} \left( \frac{V_G}{f_{\min} D_T} \right)^{2.7} \sigma_B^2 \quad (3)$$

by Niemann (1980)

in which  $\sigma_B$  and  $\sigma_R$  are the background and resonance components;  $V$  is velocity at 10 meters high;  $V_G$  is the gradient velocity;  $f_{\min}$  is the fundamental frequency;  $D_T$  is the throat diameter of HCTs;  $L$  is the turbulence length scale;  $K(\zeta)$  contains the influence of damping.

Besides the wind velocity, other factors also attracted attentions. Singh and Gupta (1976) considered the factors of latitude distribution of mean and fluctuating pressures, correlation, tower height, terrain roughness which determines the turbulence intensity and power law exponent. Besides, Lu *et al.* (1982) considered more parameters including the structural boundary condition and damping ratio. However, both of the studies just list the corresponding gust response factor for each parameter value, which couldn't describe the influence mechanism clearly. Ke *et al.* (2015, 2018c) also conducted analysis of wind-induced responses of HCTs with different feature sizes and damping ratios. It should be noted that the above four studies all taking two or three HCTs as examples to analysis the influence of tower height. Actually, the tower height is a comprehensive factor for wind responses, because it involves many factors above, for example the frequencies, mode shapes and correlation.

The present study would elaborate the influence mechanisms from four factors, including the fundamental frequency  $f_{\min}$ , modal damping ratio  $\zeta$ , wind velocity  $V$  and meridian correlation. There are also some other factors but not considered here for certain explanations. As stated above, the representative structure dimension, such as the total height  $H$  or throat diameter  $D_T$  or diameter at other certain location, is a comprehensive factor for wind responses and couldn't be discussed independently here. There is also convenience that just one HCT and corresponding wind tunnel test could provide necessary information for the four factors above. Another, terrain roughness is also an important factor which determines the gradient height, the power-law index  $\alpha$  and the turbulence intensity, but almost all HCTs are located in open country, which belongs to Type B terrain according to Chinese code GB 50009 or Category II according to Germany code VGB-R 610Ue, or Type C terrain according to American code ASCE7, and thus the wind properties are determined, or not the prime variable, in structural design. Unless the specifications in codes are redefined, there is no practical application for other terrain roughness. Therefore, factors of structure dimension and terrain roughness would not be discussed below.

For the factors of latitude wind pressure distribution and the latitude correlation, these two parameters could be easily got from wind tunnel tests, and the results got from different scholars always share the same pattern (Zhang *et al.* 2013), so they are not included as well. On the other hand, study on the meridian correlation owns its practical value. Most wind pressure tests on prototype structures and some wind tunnel tests fixed up only one or quite limited section of taps, and the exact meridian correlation couldn't be obtained. Consequently, perfect correlation (Steinmetz *et al.* 1978, Basu and Gould, 1980) or assumed correlation (Abu-Sitta and Hashish, 1973, Hashish and Abu-Sitta 1974) was employed in some studies. Therefore, it's necessary to compare the results got from the perfect and true partial correlation.

In present study, not only the gust response factors, i.e.  $G_s$ , are provided for different parameter values of each factor, but close attention was paid on the background and resonance component  $\sigma_B$  and  $\sigma_R$ , and their contributions to the total rms value  $\sigma_T$ . Therefore, this would provide a comprehensive and systematical understanding on the influence mechanism of each factor. Another, this study is the extension of a former study (Zhang *et al.* 2017) which focused on the dynamic calculation in time domain, features of wind dynamic responses and the equivalent static wind loads of the same HCT.

## 2. Wind effects of the HCT using design parameters

### 2.1 Structural and wind parameters of the HCT

The HCT selected for the following study is shown in Fig. 1, which is in the preliminary design stage of an inland nuclear power plant of China. The HCT was modeled by ANSYS for the dynamic properties and the following dynamic calculation. The shell was modeled by element Shell181; the upper cornice and the supporting columns were modeled by element Beam188. The tower shell was meshed into 36 elements along meridian direction non-uniformly and 72 elements along latitude direction uniformly respectively. This meshing is a balance of calculation efficiency and precision after numerous trials. The top stiffening ring is meshed into 72 beam elements as well to match with the shell meshing. Another, each column was meshed into 8 elements. The columns were constrained at the bottom to exclude the soil-structure interaction.

The internal forces in the tower shell are shown in Fig. 2. The X and Y directions represent the latitude and meridian directions respectively. There are axial force and moment in each direction. The axial force is positive for tension and negative for compression; moment is positive if the outside surface is tension and negative if the inside surface is tension. Moreover, subscript T and C are used to represent the positive and negative axial force respectively; subscript O and I represent the positive and negative moment similarly. The internal forces concerned in structural design and scientific research are always the axial forces and moments, so the shear force and torsion wouldn't be discussed as usual. Displacement, noted as  $U$ , is also a concern even if it has no direct influence for structural

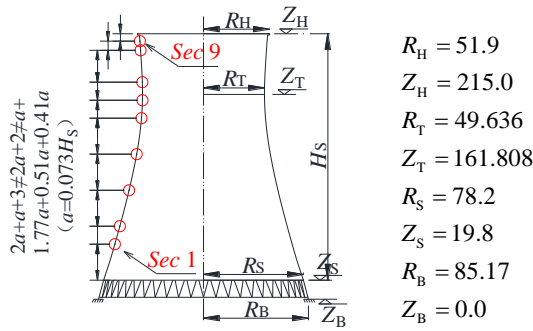


Fig. 1 Geometry of the HCT and tap locations of the model (unit: m)

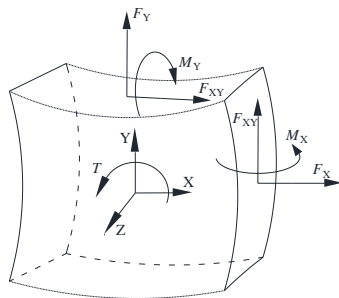


Fig. 2 Internal forces in a shell element

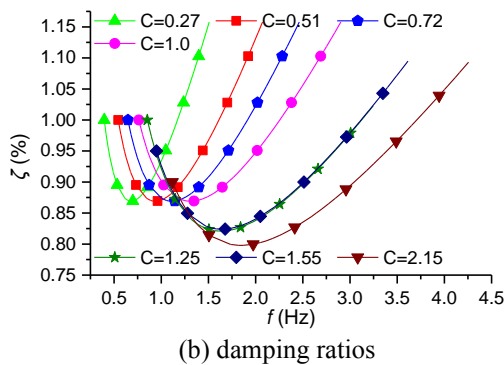
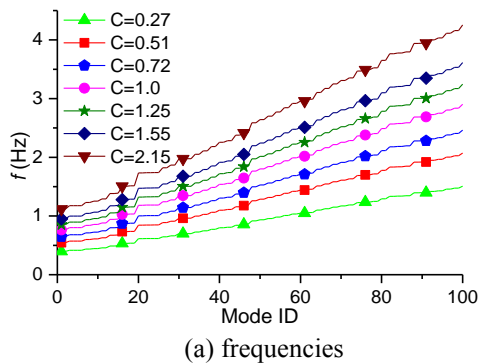
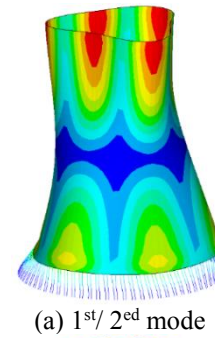


Fig. 3 Frequencies and damping ratios of the top 100 modes

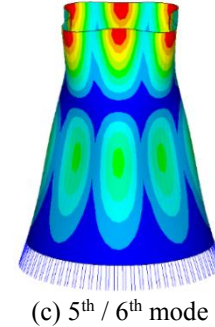
design, and it's also distinguished by subscript O and I for outward (negative) or inward (positive) displacement. Frequencies of the top 100 modes show a linear increase roughly from 0.763Hz to 2.903Hz (line C=1.0 in Fig. 3, other lines are explained in section 3.1) and it can be seen



(a) 1<sup>st</sup>/ 2<sup>nd</sup> mode



(b) 3<sup>rd</sup> / 4<sup>th</sup> mode



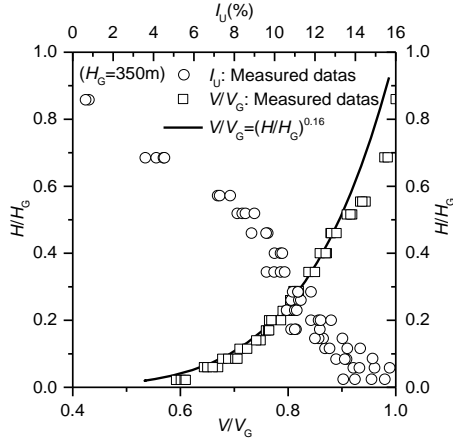
(c) 5<sup>th</sup> / 6<sup>th</sup> mode

Fig. 4 The top six modes of the HCT

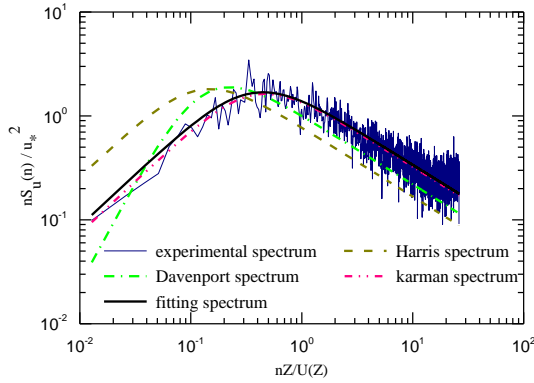
clearly that HCTs have a very dense spectrum of natural frequencies. Another, most of the modes are coupling of latitude and meridian waves, as shown of the top six modes in Fig. 4.

The wind environment is Type B terrain according to code GB 50009 of China. The basic wind velocity of the site, namely the yearly-maximum 10-min averaged mean wind velocity at 10m height corresponding to 50-year return period is  $V_0=24.5\text{m/s}$  for Type B terrain, which is also the minimal basic velocity according to code GB 50009. The mean wind velocity on the HCT top is  $V_H=40\text{m/s}$  according to the power-law index  $\alpha=0.16$  for mean wind velocity profile. The wind pressure field was obtained through rigid model test in wind tunnel TJ-3 at Tongji University, with a dimension scale  $\lambda_L=1/200$ . The wind environment of Type B terrain was simulated and Fig. 5 presents the simulated mean velocity and turbulence intensity profiles and fluctuating wind spectra in TJ-3. More detailed information about the experiment could be found in Ref. (Zhang *et al.* 2013, Zhang *et al.* 2017).

The experiment velocity is  $V_E=10\text{m/s}$  on the model top, i.e. the velocity scale  $\lambda_V=1/4$  and time scale  $\lambda_T=1/50$ . The surface roughness of the model was changed to compensate the Reynolds number effect. The taps located on 9 sections (Fig. 1) and each section has 36 taps distributed uniformly.

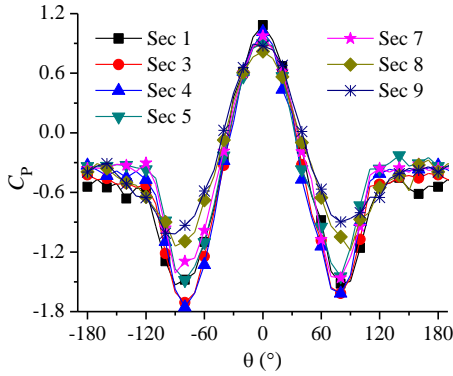


(a) mean velocity and turbulence intensity profiles

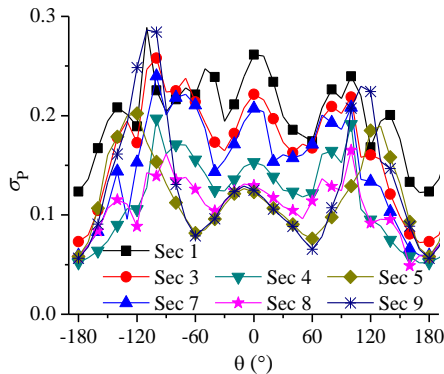


(b) power spectra function of along wind component

Fig. 5 Wind field properties simulated in wind tunnel TJ-3



(a) mean pressure distribution



(b) fluctuating pressure distribution

Fig. 6 Wind pressure distributions on different sections

The internal pressure was not measured because it is not incorporated in the reinforcement design in Chinese code. Wind pressures were measured simultaneously at all taps using the multi-channel simultaneous fluctuating pressure measurement system. The sampling frequency was 312.5Hz and the record lasts 19.2s, i.e. 6000 time-steps. Fig. 6 shows the mean and fluctuating (i.e. rms) wind pressure coefficients along latitude, noted as  $C_p$  and  $\sigma_p$ , and these results are in good agreement with results of other studies. The coefficients at each section were normalized by the mean velocity pressure at its elevation.

## 2.2 Dynamic calculation method

Based on the FE model and wind pressure field history, dynamic calculation in time domain could be conducted. Zhang *et al.* (2017) has presented the calculation method and parameters in detail, but a brief description is still necessary here. Rayleigh damping was adopted and the modal damping ratio  $\zeta=1\%$  was assumed for the 1<sup>st</sup> and the 70<sup>th</sup> modes according to some tests on prototype structures. Finally, the modal damping ratio varies from 0.8% to 1.3% for the top 100 modes, as shown by line  $C=1.0$  in Fig. 3. The wind pressure field history got from the test was scaled to get the load history on the prototype structure and then expanded by POD method to apply on nodes of the FE model. A time-domain approach was employed in the dynamic calculation, using both the implicit direct integration method and mode-superposition method. The results got from the two methods compared quite well with each other so just the former results are presented. The solution of the dynamic equations of equilibrium was obtained by Newmark- $\beta$  method and  $\beta=1/4$  was used which yields the constant average acceleration method. Another, the integration time step  $\Delta t=1/37.5s$  was specified, covering the top 53 modes, according to the comparison of the results obtained using a smaller value of  $\Delta t$  to assure that results were insensitive to further reduction of  $\Delta t$ .

What should be emphasized here is the method how to separate the background component  $\sigma_B$  and resonant component  $\sigma_R$  from the total rms value  $\sigma_T$ , because  $\sigma_B$  and  $\sigma_R$  are the crucial indexes to analyze the influence mechanism in present study. For wind-induced dynamic calculation in frequency domain, accurate  $\sigma_R$  could only be obtained for SDOF model (Eq. (4)~ Eq.(5)); the  $\sigma_B$  and  $\sigma_T$  for SDOF model are also listed here as well (Eq. (6)~ Eq.(8))

$$m\ddot{y}(t) + c\dot{y}(t) + ky(t) = p(t) \quad (4)$$

$$\sigma_R^2 = \frac{1}{k^2} \frac{\pi f_0 S(f_0)}{4\zeta} \quad (5)$$

$$\sigma_B^2 = \frac{1}{k^2} \int_0^\infty S(f) df \quad (6)$$

$$\sigma_T^2 = \int_0^\infty S(f) |H(f)|^2 df \quad (7)$$

$$|H(f)|^2 = \frac{1}{k^2} \cdot \frac{1}{[1 - (f/f_0)^2]^2 + 4\zeta^2 (f/f_0)^2} \quad (8)$$

in which  $m$ ,  $c$  and  $k$ =the mass, damping and stiffness respectively;  $y$ ,  $\dot{y}$  and  $\ddot{y}$  =the displacement, velocity and acceleration of the mass; and  $p(t)$  is the time-varying stochastic load;  $S(f)$  is the power spectrum of  $p(t)$ ;  $f_0$  is the frequency of the SDOF model.

For real structures which inevitably belong to MDOFs, the  $\sigma_B$  and  $\sigma_T$  can also be acquired in frequency domain by means of mode-superposition method: they are not listed here for their complicated expressions. However, there is no explicit expression for the resonant component  $\sigma_R$  for MDOF structures. Therefore, the  $\sigma_B$  and  $\sigma_R$  are always divided approximately from the response spectrum at certain frequency, for example 0.2Hz or 0.3Hz as used by Armit (1980). However, this method would not be valid if the  $f_{min}$  is very small, or the coupling component between  $\sigma_B$  and  $\sigma_R$  couldn't be ignored.

On the other hand, the background and resonant responses could be obtained easily in time domain calculation, no matter SDOF or MDOF structures. Taking the SDOF for an example as well, ordinary dynamic calculation would only get the total response history  $y_T(t)$  (Eq. (4)). When a quasi-static calculation in history is conducted meanwhile, the background response history  $y_B(t)$  would be obtained (Eq.(9)). If subtracting  $y_B(t)$  from  $y_T(t)$ , what left would be the pure resonant response history  $y_R(t)$ . Obviously, this method is valid not only for the displacement responses, but also valid for the internal forces. For any response, the corresponding power spectrum of  $y_R(t)$  would almost be zero except at the frequencies of the structures, as shown in Fig. 7 below, which is the expected reflection of the resonant component.

$$ky_B(t) = p(t) \tag{9}$$

$$y_R(t) = y(t) - y_B(t) \tag{10}$$

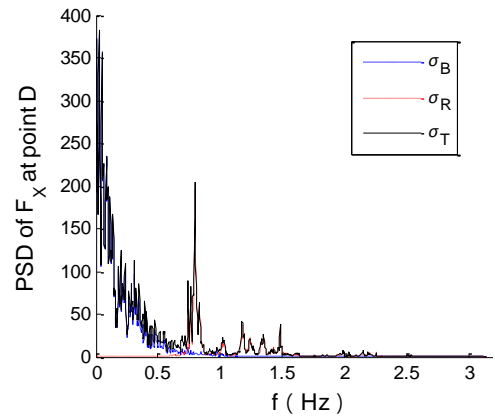
There is still one thing should be noted about the separating method in time domain: the coupling component between the background and resonant components, noted as  $\sigma_{BR}$  and expressed by

$$\sigma_T = \sqrt{\sigma_B^2 + \sigma_R^2 + \sigma_{BR}} \tag{11}$$

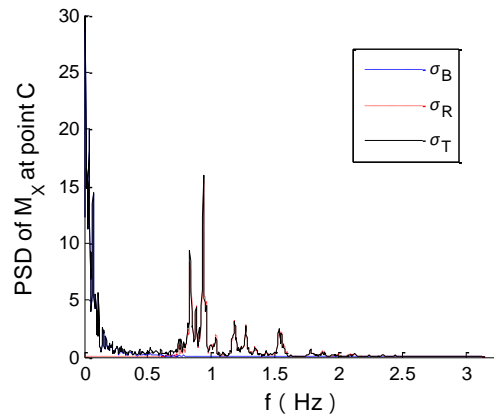
This question has been discussed by Ke *et al.* (2012) in frequency domain. The separating method in time domain would bring coupling component as well, because the  $y_B(t)$  and  $y_R(t)$  both have power spectrums around the structural frequencies. However, the coupling component of HCTs are very little and could be ignored, as illustrated in Fig. 8 and Table 1 bellow. It also could be identified from Fig. 7 that the resonant components of the three internal forces are contributed from different frequencies: 0.7Hz~0.8Hz for  $F_x$  at point D, 0.7Hz~0.9Hz and 1.2Hz~1.4Hz for  $F_y$  at point B, 0.8Hz~1.0Hz for  $M_x$  at point C. The obvious demonstration of the contributions from different modes for different responses origins from the mode shape characteristics, and it also demands a careful decision on the dynamic calculation parameters to cover sufficient mode numbers.

### 2.3 Wind effects for design parameters

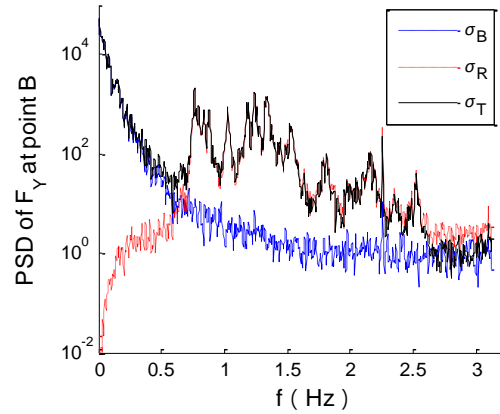
The dynamic effect is always expressed by gust response factor  $G$  noted as



(a)  $F_x$



(b)  $M_x$



(c)  $F_y$  (in log coordinates)

Fig. 7 Power spectrums of three internal forces

$$G = 1 + \text{sign}(\bar{A})g \frac{\sigma_T}{A} \tag{12}$$

in which  $\bar{A}$  is the mean value and  $g$  is the peak factor.

Obviously, each response has its own gust response factor  $G$ , which means  $G$  varies with locations and responses such as internal forces and displacements, as shown below in Fig. 9. This brings great obstacle for its direct application in structural design and pursuing the equivalent static wind load is still an important mission.

The wind effects under the design parameters should be presented firstly before the influence mechanism analyses.

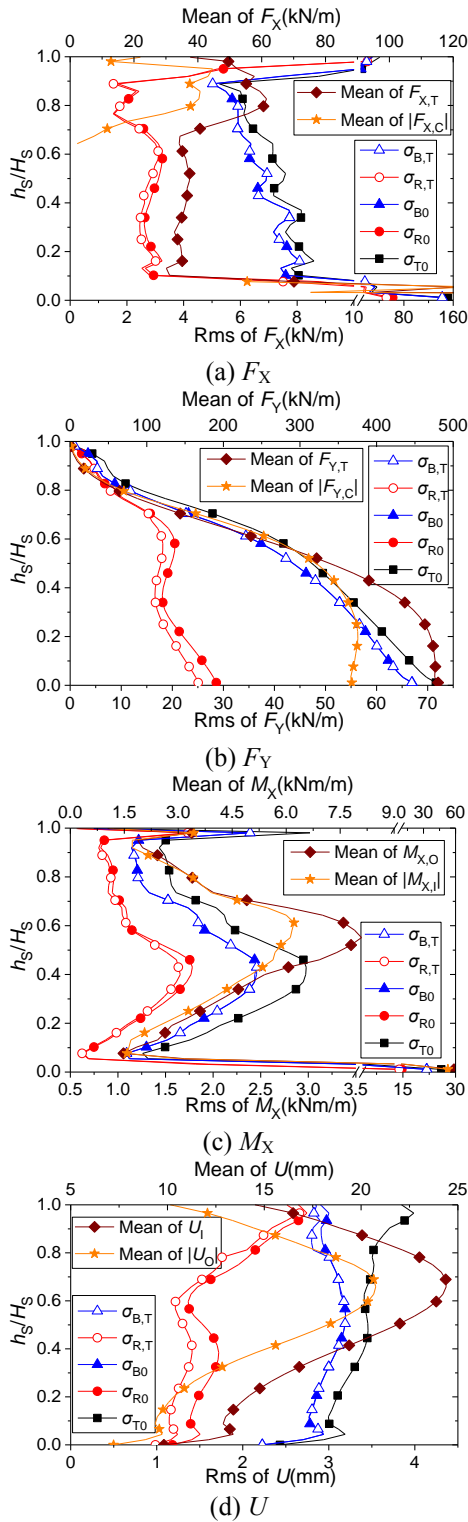


Fig. 8 Mean and fluctuating responses

The design parameters including the original structure, modal damping ratio  $\zeta=1\%$ ,  $V_0=24.5\text{m/s}$  (i.e.  $\lambda_T=1:50$  and  $\lambda_V=1:4$ ) and the whole surface wind pressure field from wind tunnel test: all of them have been presented in section 2.1. This condition is referred as benchmark condition for other parameters. The representative results of the concerned responses under wind loads in structure design are shown in Fig. 8 and Fig. 9. Detailed discussion of these

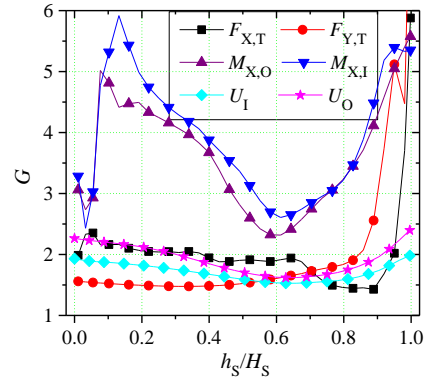


Fig. 9 Meridian distributions of gust response factors for different responses

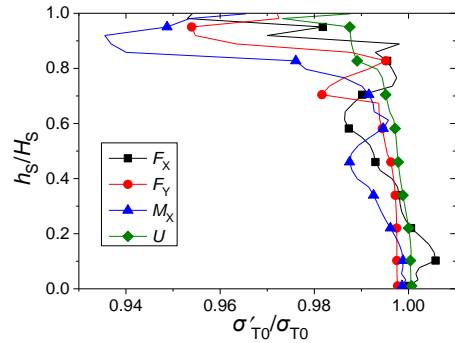


Fig. 10 Demonstration of the coupling effect between  $\sigma_R$  and  $\sigma_T$

results has been presented by Zhang *et al.* (2017), but the following information should be stated here again. First, the mean value  $\bar{A}$ , background component  $\sigma_{B0}$ , resonant component  $\sigma_{R0}$  and the total rms values  $\sigma_{T0}$  plotted in Fig. 8 are the maximum amplitude along latitude, but these values may not coincide at the same latitude location; the background and resonant components  $\sigma_{B,T}$  and  $\sigma_{R,T}$  are picked up at the very location where  $\sigma_{T0}$  exists. Second, the peak factor  $g$  used for the gust response factor  $G$  is  $g=3.75$  for meridian internal forces and displacement,  $g=4.5$  for latitude internal forces as explained by Zhang *et al.* (2017).

As far as the coupling component, if it is ignored and employing the following equation to calculate the total rms

$$\sigma_{T0}' = \sqrt{\sigma_{B,T}^2 + \sigma_{R,T}^2} \quad (13)$$

the result would be very close to the  $\sigma_{T0}$  and the ratio of  $\sigma_{T0}'/\sigma_{T0}$  is also shown in Fig. 10. As stated above, the coupling component for HCTs could be ignored. That's because the wind energy mainly concentrates below  $0.3\text{Hz}$  and the  $f_{\min}$  is  $0.763\text{Hz}$  for this HCT, which restrains the coupling component fundamentally. Moreover, the coupling component could still be neglected even  $f_{\min}$  is adjusted to  $0.396\text{Hz}$  whose results are presented in section 3.1.

Generally speaking, the gust effects of the axial forces and displacement are always much smaller than the latitude moment in region  $h_s/H_s < 0.8$ ; in top shell, the gust effects of every responses all exhibit great increase for the decreasing mean value. It's clear that the background component  $\sigma_B$  is

dominating in the total rms value  $\sigma_T$ , especially for  $F_X$ ,  $F_Y$  and  $U$  in the middle and lower shell. Another, the coincidence of line  $\sigma_{B0}$  and line  $\sigma_{B,T}$  indicates  $\sigma_{B0}$  and  $\sigma_{T0}$  locate at the same latitude location. This could also be explained by the dominance of the background component  $\sigma_B$ . For the resonant component  $\sigma_R$ , however, there is always gap between the two lines, which means the  $\sigma_{R0}$  and  $\sigma_{T0}$  wouldn't locate at the same latitude location. Yet the gap is small, implying the resonant component  $\sigma_{B,T}$  where  $\sigma_{T0}$  exists is still notable compared with  $\sigma_{B0}$ .

If the resonant effects are ignored, the total rms value of  $F_{Y,T}$  would decrease about 5%, 5%~20% and 20% for region  $h_s/H_s < 0.5$ ,  $0.5 < h_s/H_s < 0.8$  and  $0.8 < h_s/H_s < 1.0$ . Although the decrease in the top is remarkable,  $F_{Y,T}$  in this region has no practical meaning for the reinforcement design and still could be neglected. However, the seemingly minor decrease in the lower and middle shell couldn't be neglected because the reinforcement amount in this region is quite sensitive to the wind induced  $F_{Y,T}$ . For the  $\sigma_{T0}$  of latitude internal forces, remarkable decreases appear also in the top region. The total rms value of  $F_{X,T}$  decreases about 5%~10% and 10%~30% for region  $h_s/H_s < 0.9$  and  $0.9 < h_s/H_s < 1.0$ , and the total rms value of  $M_X$  decreases about 18%~23% and 20%~30% for region  $h_s/H_s < 0.7$  and  $0.7 < h_s/H_s < 1.0$ . However, the wind induced latitude internal forces determine the latitude reinforcement of the top shell together with temperature and dead weight, so the resonant effects couldn't be neglected. Another, even if the resonant effects are ignored, the gust response factor for  $M_X$  still lies between 2.0 and 4.0, which is close to the result got from Ref. (Abu-Sitta and Hashish, 1973), i.e. 2.0 ~ 3.0.

It is evident that each response at each location of the tower shell would show different sensitivities to the structural and wind parameters, and it's impossible to select all responses for the following analysis. Even the internal forces in Fig. 8 don't determine the reinforcement in the whole height: each internal force has its own dominating area according to Zhang *et al.* (2017). For example, the dominating area of  $F_{Y,T}$  is in the middle and lower shell,  $F_{X,T}$  in the top shell and  $M_X$  in the whole shell. Therefore, for clear illustration of the influence from various factors, several representative responses at certain locations were selected for the following analysis, as listed in Table 1. By the way, some corresponding results for other damping ratios are also listed here for following comparison.

The four locations in Table 1 are Point A:  $h_s/H_s=0.19$ ,  $\theta=0^\circ$ ; Point B:  $h_s/H_s=0.49$ ,  $\theta=0^\circ$ ; point C:  $h_s/H_s=0.70$ ,  $\theta=-95^\circ$ ; point D:  $h_s/H_s=0.92$ ,  $\theta=-95^\circ$ . These locations were selected after careful consideration in order to present a reasonable study result. The selection of meridian locations of these points have been explained before. The latitude locations are selected in the light of the latitude distributions of the mean and rms values, as exhibited by Zhang *et al.* (2017). For example, the maximum latitude mean and total rms values of  $F_Y$  both located at  $\theta=0^\circ$  for  $h_s/H_s=0.19$  and  $h_s/H_s=0.49$ ; locations of the maximum latitude mean and total rms values of  $F_X$  not coincide for  $h_s/H_s=0.70$  and  $h_s/H_s=0.95$  but the mean and total rms values at  $\theta=-95^\circ$  are very close to the corresponding maximum values; the situation of  $M_X$  is similar to the  $F_X$ .

Table 1 Responses at certain locations for different damping ratios

Internal force	Locations	$\bar{A}$	$\sigma_B$	$\zeta=1\%$		$\zeta=3\%$		$\zeta=5\%$	
				$\sigma_R$	$\sigma_T$	$\sigma_R$	$\sigma_T$	$\sigma_R$	$\sigma_T$
$F_{Y,T}$ (kN/m)	A	471.35	58.83	19.60	63.44	11.58	61.43	9.10	61.00
	B	346.23	43.85	17.19	47.53	9.75	45.36	7.38	44.91
$F_{X,T}$ (kN/m)	C	37.83	5.90	2.43	6.45	1.53	6.16	1.24	6.09
	D	49.30	7.02	3.81	8.13	2.45	7.58	2.02	7.44
$M_X$ (kNm/m)	A	-1.44	0.93	1.31	1.58	0.75	1.16	0.56	1.05
	B	-5.07	1.54	1.82	2.37	1.02	1.83	0.77	1.70
	C	0.67	1.31	1.18	1.75	0.74	1.49	0.61	1.43
	D	0.75	1.00	0.96	1.43	0.65	1.23	0.56	1.18

It can be seen that the total rms values are much less than the corresponding mean values for  $F_{Y,T}$  in the benchmark condition, i.e.  $\sigma_T/\bar{A}=1/7.36$ ; this ratio for  $F_{X,T}$  is just a little bigger, i.e.  $\sigma_T/\bar{A}=1/5.96$ ; whereas the total rms value and the mean value of  $M_X$  are of the same order of magnitude, even for greater damping ratios. These results are in good consistent with Fig. 8 and explain the gust response factors in Fig. 9. Moreover, in the benchmark condition, the resonant components are much less than the background components for  $F_{X,T}$  and  $F_{Y,T}$  both. The ratios of  $\sigma_B/\sigma_R$  lie between 1.8 and 3.0, and this ratio for  $F_{Y,T}$  is also a little less compared with  $F_{X,T}$ . It means the background components are dominating in the total rms values for  $F_{X,T}$  and  $F_{Y,T}$ : their ratios of  $\sigma_B/\sigma_T$  lie between 85% and 95%. For  $M_X$ , nevertheless, its background and resonant components are very close to each other, i.e.  $\sigma_B/\sigma_R$  is approximately equal to 1.0 and  $\sigma_R$  is even bigger than  $\sigma_B$  at certain locations, which explains the remarkable total rms responses and the gust response factor of  $M_X$ .

The differences of gust effects of the three internal forces also reflect the structural mechanism under wind loads which is illustrated by their influence functions under surface pressure (Fig. 11).  $F_X$  and  $M_X$  at a certain location is mainly determined by its surrounding local pressure, but  $F_Y$  is determined by the whole shell pressure: therefore, the former could be called as local internal forces and the latter as global internal force. As a result, the gust effects of  $F_Y$  would be smoothed greatly for lower correlation over a large area of the wind pressure.  $F_X$  and  $M_X$  are both local internal forces, but their differences of gust effects could be explained by the local influence functions and wind pressure correlation in meridian direction. The local influence function of  $M_X$  along meridian direction is always negative, but varies quickly from positive to negative and to positive again for  $F_X$ . Another, the local correlation along meridian is usually very high. Consequently, the high local correlation combined with influence function with the same sign gives birth to high background component and ultimately remarkable gust response factor, exactly as  $M_X$ , and on the contrary situation is  $F_X$ .

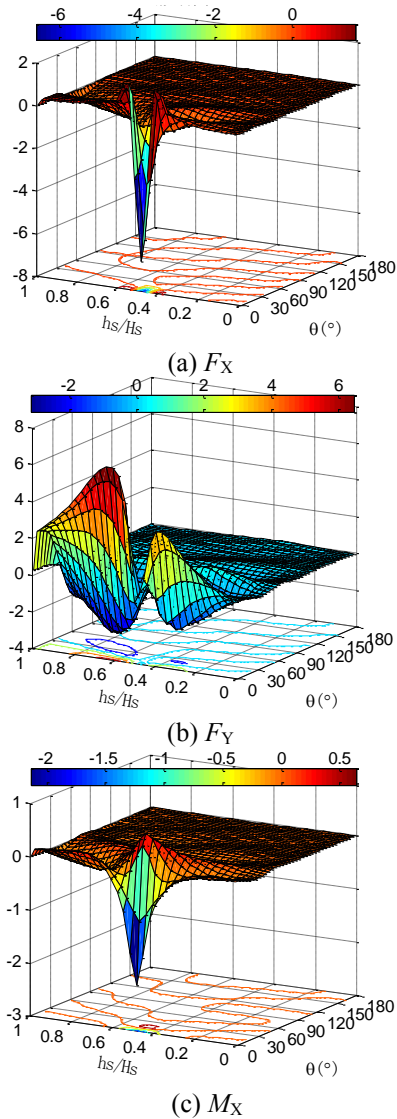


Fig. 11 Influence functions of internal forces at point B

### 3. Influences from different factors

#### 3.1 Fundamental frequency

It is clear that the fundamental frequency  $f_{\min}$  is the most critical factor for wind induced dynamic effects. Usually, this factor is studied through several HCTs with different  $f_{\min}$ , but the variation of  $f_{\min}$  is very limited and involves inevitably other factors like the structure dimension, correlation and so on. In this study, a new method was proposed in which only one HCT was selected to ensure the structure dimension and correlation unchanged but the elastic modulus  $E$  of the HCT was altered by a coefficient  $C$  (Table 2) to get a series of structures with different  $f_{\min}$ .

What should be mentioned is that adjusting the meridian curve or thickness could also change the  $f_{\min}$ , but altering the elastic modulus  $E$  is the most efficient way. Noh and Lee (2012) altered the meridian curve of a 150m HCT to get different  $f_{\min}$  and analyzed the sensitivity to wind excitation, but the  $f_{\min}$  varies only from 0.587Hz to 0.752Hz for the total generated 32 curves. The thickness of HCT in Ref. (Zhang *et al.* 2013) was altered from 201mm to

Table 2  $f_{\min}$  for different elastic modulus coefficients

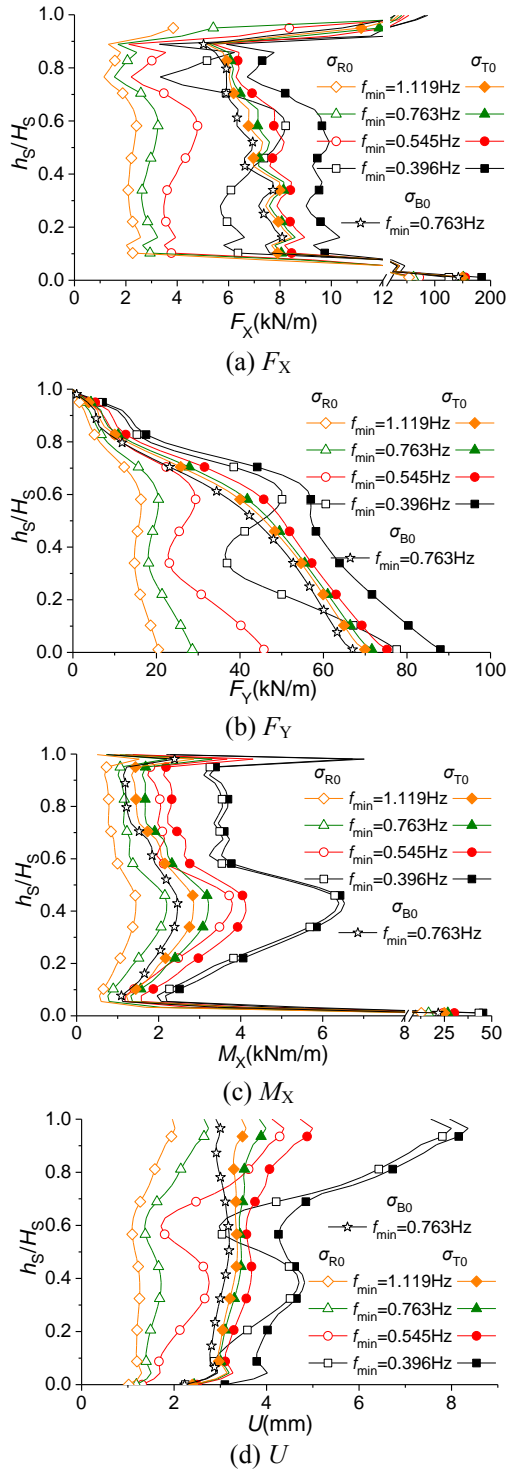
Coefficient $C$	$f_{\min}$ (Hz)	Integration time step $\Delta t$ (s)	The upper frequency covered for $\Delta t$ (Hz)	The number of modes covered for $\Delta t$
0.27	0.396			>100
0.51	0.545	1/37.5	1.875	87
0.72	0.647			67
1.0	0.763			53
1.25	0.853	1/43.8	2.188	55
1.55	0.950	1/50	2.5	59
2.15	1.119	1/56.25	2.813	53

341mm, and the  $f_{\min}$  varies only from 0.869Hz to 0.904Hz. It can be seen from Table 2 and Fig. 3 that the  $f_{\min}$  of this HCT varies from 0.396Hz to 1.119Hz, covering all the  $f_{\min}$  of large HCTs reported. Another, the  $f_{\min}$  is approximately in proportion to  $C^{0.5}$ , because  $C$  is the index of the global structural stiffness.

One more advantage for the altering of elastic modulus  $E$  is it wouldn't change the internal forces under static load because the stiffness distribution of the HCT, which is a statically indeterminate structure, always maintain the same. This implies that the mean component and background component of internal forces under fluctuating wind loads would neither vary with elastic modulus. Then, only the resonant component and the total rms value vary with elastic modulus due to the alternation of  $f_{\min}$ , and they are also the prime concerns for the factor of  $f_{\min}$ . Of course the displacement would vary with elastic modulus and stiffness even under static load, but the product of displacement and the coefficient  $C$  still always maintain the same. So, the displacements list below, including all the components, were multiplied by the coefficient  $C$  to compensate the influence just from stiffness, but the coefficient  $C$  no longer appear explicitly in the following expressions and notations. In this way, the resonant component and the total rms value of displacement list below also only influenced by the  $f_{\min}$ . Consequently, this method may be most appropriate one to study the influence of  $f_{\min}$  on the wind induced gust effects.

Another, some other measures are needed for accurate calculation of the gust effects in the variation of  $f_{\min}$ . First, the integration time step  $\Delta t$  should also be adjusted correspondingly (Table 2) to cover sufficient modes in the dynamic calculation. Second, the parameters of Rayleigh damping was also adjusted to ensure the modal damping ratio for modes under 1.9Hz are all near 1% for each coefficient  $C$  (Fig. 3 (b)).

As stated above, only the resonant components and the total rms values are shown in Fig. 12, the background components of the original structure are also plotted for convenient comparison. It is shown clearly that the resonant components increase greatly when  $f_{\min}$  is below 0.7Hz, and the great increase of total rms values occur just when  $f_{\min}$  is below 0.5Hz as the contribution from the resonant components is limited. Because the increase of total rms value origins completely from the resonant component and  $f_{\min}$  is the critical factor for the resonant component, some


 Fig. 12  $\sigma_{R0}$  and  $\sigma_{T0}$  for different fundamental frequencies

researchers have proposed some expressions for the resonant component (Eq.(1), Eq.(2), Eq.(3)). However, evident discrepancy could be found in the expressions about the relationship between the resonant component and  $f_{\min}$ : the resonant component is proportional to  $1/f_{\min}^{3.4-3.75}$ ,  $1/f_{\min}^2$  and  $1/f_{\min}^{1.35}$  according to Eq.(1) ~ Eq.(3) correspondingly.

It should be noted that these expressions are fitted from experiments (Eq.(1) and Eq.(2)) or calculations (Eq.(3))

because there are always many modes contributing to the resonant component and it's seemingly almost impossible to form a practical and simple expression theoretically. Another, these expressions are all aiming at the resonant component of  $F_{Y,T}$  at certain locations which are not given clearly. Maybe the difference of selected locations is part reason for the discrepancy as well.

According to the results in Fig. 12, a new fitted graph could be plotted (Fig. 13) for the resonant component, against a new parameter

$$RP = \frac{1}{f_{\min}} \cdot \left( \frac{1}{f_{\min}} - \frac{1}{2} \right) \quad (14)$$

in which  $\frac{1}{f_{\min}}$  denotes the contribution from one single

mode and  $\frac{1}{f_{\min}} - \frac{1}{2}$  denotes the contribution from the frequency scope, i.e. from  $f_{\min}$  to 2.0Hz. The upper frequency limit 2.0Hz is got from Fig. 7. Then, the product of multiplication could be used as an index for the resonant component. Of course when  $f_{\min}$  of a HCT is greater than 2.0Hz, its resonant component could be neglected.

It is evident that  $\sigma_{R0}$  and  $RP$  are linear approximately for all responses at any locations, just the slopes exhibit certain discrepancy for different responses. Statistically, the slopes are 0.45, 0.41, 0.36 and 0.32 for  $M_X$ ,  $U$ ,  $F_Y$  and  $F_X$  respectively. Considering the joint action of  $F_X$  and  $M_X$  and the significance of  $F_Y$  in structural design, a single slope 0.4 could be used for all responses. So, the final expression could be written as

$$\frac{\sigma_{R0}}{\sigma_{R0}(f_{\min}=0.763)} = 0.4(RP - 1) \quad (15)$$

It can be seen from Fig. 14 that the gust responses factors  $G_s$  show inconspicuous variation when  $f_{\min}$  is greater than 0.7Hz for all responses except  $M_X$ , whose  $G$  still shows certain increase when  $f_{\min}$  decrease from 0.9Hz to 0.7Hz. When  $f_{\min}$  is less than 0.5Hz, the  $G_s$  would increase quickly for all responses. This also imply that the  $f_{\min}$  had better be greater than 0.7Hz to exhibit less sensitivity to the gust wind. Actually, the  $f_{\min}$  is always bigger than 0.7Hz for HCTs over 200m high, for example 0.74Hz for the Frimmersdorf HCT which is 200m high (Busch *et al.* 1998), 0.808Hz for a planning HCT which is also 200m high (Zou *et al.* 2013), and this HCT in planning as well. Moreover, the  $f_{\min}$  could be optimized to some extent by adjusting the meridian curve (Noh and Lee 2012).

### 3.2 Damping ratio

Damping ratio is an important factor for structural dynamic responses. According to the common damping ratio value of concrete structures,  $\zeta=3\%$  and  $5\%$  were used for this study besides the base value  $\zeta=1\%$ .

It is well known that the damping ratio just determines the resonant component  $\sigma_R$  and further the total rms value  $\sigma_T$ , but not the background component  $\sigma_B$ , which is also expressed in Eq. (4)~Eq.(10). Therefore, the corresponding

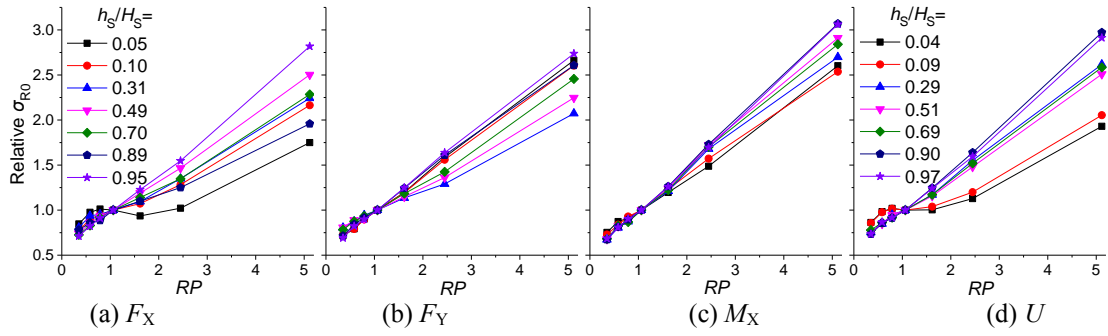


Fig. 13 Relationships between  $\sigma_{R0}$  and  $RP$  for different responses

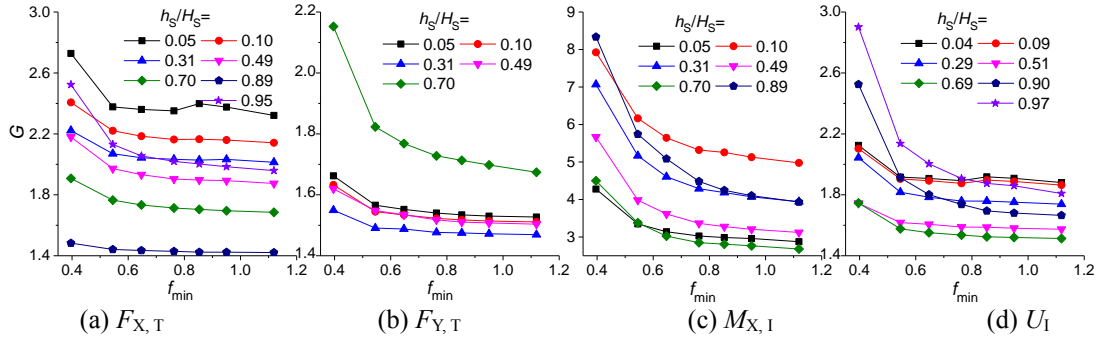


Fig. 14 Relationships between  $G$  and  $f_{min}$  for different responses

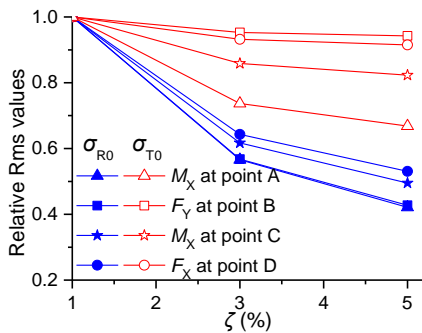


Fig. 15 Relative gust responses for different damping ratios

$\sigma_R$  and  $\sigma_T$  of three modal damping ratios were listed in Table 1 together for convenient comparison. It's shown clearly from Table 1 and Fig. 15 that the resonant components of every responses decrease nearly at the same rate with the increase of  $\zeta$ , and the decrease rate could be expressed approximately by

$$\frac{\sigma_R(\zeta_1)}{\sigma_R(\zeta_2)} = \sqrt{\frac{\zeta_2}{\zeta_1}} \quad (16)$$

which is deduced from Eq. (5). For the total rms value  $\sigma_T$ , the decrease rates of every responses disagree with each other on account of the different contributions from  $\sigma_R$  as stated in Section 2.3. As a result, the total rms values of  $F_X$  and  $F_Y$  show little sensitivity to the damping ratio  $\zeta$  and  $M_X$  is quite sensitive to  $\zeta$ . What should be noted again is the two latitude internal forces  $F_X$  and  $M_X$  of wind always work together for the latitude reinforcement, and consequently their sensitivity to damping ratio would be neutralized to some extent. Moreover, the sensitivity would be further

relieved in consideration of the load effects combination of wind, dead weight and temperature. So, it's recommended that  $\zeta=1\%$  is used in dynamic calculation and structural design of HCTs for reasons from three aspects: results from prototype tests, the sensitivities of dynamic responses and a little conservative design.

### 3.3 Wind velocity

Although the resonant effects at the design wind velocity  $V_0=24.5\text{m/s}$  are quite limited, the higher velocity would increase the resonant effects because the wind spectrum tends to higher frequency domain. Based on the wind tunnel test, the  $\lambda_V$  and  $\lambda_T$  could be adjusted to get different wind velocities for the prototype structure, and the product of  $\lambda_V$  and  $\lambda_T$  should remain unchanged, i.e.  $\lambda_V\lambda_T=\lambda_L=1/200$ , in the adjustment. Following this regulation, five new groups of  $\lambda_V$  &  $\lambda_T$  were selected (Table 3) for analyze the influence of wind velocity, as shown in Fig. 16. It should be noted that with the variation of wind velocity the Reynolds number also changed and this would change the wind pressure distributions more or less. However, for HCTs, the Reynolds number is always beyond  $0.8 \times 10^8$  and there is no strong evidence how the Reynolds number would affect the wind pressure. So, the wind pressure remain the same as shown in Fig. 6 in the variation of wind velocity.

It is evident that all the response components, including  $\bar{A}$ ,  $\sigma_B$ ,  $\sigma_R$  and  $\sigma_T$  would increase with  $V^2$  linearly even if the wind spectrum doesn't vary with wind velocity. In this study, however, only  $\bar{A}$  and  $\sigma_B$  increase with  $V^2$  linearly, and whereas the  $\sigma_R$  and  $\sigma_T$  would increase much quickly. It means that the additional increase of  $\sigma_R$  and  $\sigma_T$  origins from the variation of wind spectrum. In order to illustrate the influence of variation of wind spectrum on  $\sigma_{R0}$  and  $\sigma_{T0}$ , i.e.

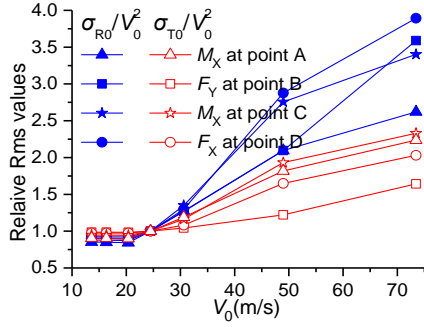


Fig. 16 Relative gust responses for different wind velocities

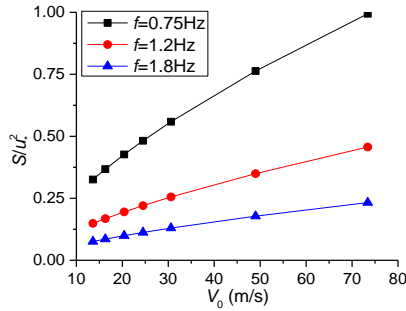


Fig. 17 Spectrum values at certain frequencies got from Davenport spectrum

Table 3  $\lambda_V$  and  $\lambda_T$  for different velocities

$\lambda_V$ & $\lambda_T$	1/2.22 & 1/90	1/2.67 & 1/75	1/3.33 & 1/60	1/4 & 1/50	1/5 & 1/40	1/8 & 1/25	1/12 & 1/16.67
$V_0$ (m/s)	13.6	16.3	20.4	<b>24.5</b>	30.6	49.0	73.4

shielding the pure influence from wind loads, the results shown in Fig. 16 are the relative value: i.e.  $\sigma_{R0}/V_0^2$  and  $\sigma_{T0}/V_0^2$ . So, the influence from velocity should be called the influence from the wind spectrum variation due to the velocity alteration.

It is expected that the  $\sigma_{R0}/V_0^2$  would increase with velocity in the whole region listed in Table 3, because the wind spectrum theoretically tends to higher frequency domain as long as the velocity increase, regardless of the start point of the increase. This can be clearly demonstrated by Fig. 17 which exhibits the increase of the spectrum values with velocity at three frequency points,  $f=0.75\text{Hz}$ ,  $1.2\text{Hz}$  and  $1.8\text{Hz}$ . The spectrum values were got from Davenport spectrum, and the frequency region  $0.75\text{Hz}\sim 1.8\text{Hz}$  is the very region where the resonant effects of this HCT come up. However, the increases of  $\sigma_{R0}/V_0^2$  and  $\sigma_{T0}/V_0^2$  begin from  $V_0>20.4\text{m/s}$  as shown in Fig. 16. That's because what used directly in the calculations are the pressure histories and pressure spectrums got from wind tunnel tests, but not the theoretical Davenport spectrum. The pressure spectrums got from wind tunnel tests no longer show sensitivity to the  $\lambda_T$  when  $\lambda_T<1/60$ . Fig. 17 is just a theoretical exhibition of the trend to higher frequency domain as long as the velocity increase.

When the  $V_0$  is greater than  $20.4\text{m/s}$ ,  $\sigma_{R0}/V_0^2$  of all responses increase approximately linearly with velocity,

especially for  $F_Y$  and especially for  $20.4\text{m/s}<V_0<49.0\text{m/s}$ . That's because the increase of the wind spectrum values at critical frequency points with velocity is also approximately linear (Fig. 17). However, as the influences from  $f_{\min}$  and  $\zeta$ ,  $\sigma_{R0}/V_0^2$  of different responses still show different sensitivities to the velocity when  $V_0>20.4\text{m/s}$ . The increase of  $\sigma_{T0}/V_0^2$  is much small compared with  $\sigma_{R0}/V_0^2$ , but the increase amplitude is still considerable for  $M_X$  and  $F_X$ , which could be explained by the contributions from  $\sigma_R$ .

Just as shown in Eq. (1) ~ Eq. (3), the resonant component  $\sigma_R$  of  $F_Y$  in the lower meridian part is proportional to  $V^{3.4\sim 3.75}$ ,  $V^4$  and  $V^{3.35}$  correspondingly. In present study, the resonant component  $\sigma_R$  of  $F_Y$  at four locations in the windward meridian line, i.e.  $h_s/H_s=0.19$ ,  $0.35$ ,  $0.49$  and  $0.70$ , is proportional to  $V^{2.85\sim 3.25}$ . The power of velocity of this study is smaller than the results from other literatures, but it could be explained by the nearly linear increase of  $\sigma_{R0}/V_0^2$  with velocity, as well as the linear increase of wind spectrum value with velocity as shown in Fig. 17. Another, the power exponent of Eq. (2) is the biggest, and the reason maybe is the group-tower effects were incorporated in the experiments which produced more resonant effects (Armitt 1980).

Of course the maximum  $V_0$  in Table 3 and Fig. 16 is too high for practical structural design. The basic velocity  $V_0$  is always less than  $35\text{m/s}$  according to code GB 50009 except in coastal areas and inland valley areas. Even when  $V_0$  increases from  $24.5\text{m/s}$  to  $40\text{m/s}$ ,  $\sigma_{T0}/V_0^2$  of  $F_Y$  at point B only increase 10%; for  $M_X$  and  $F_X$  at other points on the other hand, their  $\sigma_{T0}/V_0^2$  increase about 30%~50%. Considering the statuses of wind induced internal forces in the load effects combination, the influences on  $\sigma_{R0}$  and  $\sigma_{T0}$  of all internal forces from wind velocity should be treated carefully in the practical structural design.

Due to the complicated influences on different responses and the same response at different locations from wind velocity and the fundamental frequency, the proposed expressions of the Eq. (1) ~ Eq. (3) might not accurate enough. The rational and practical way for structural design is performing the dynamic calculation to obtain the actual dynamic responses. This idea is not as complicated as it sounds for three reasons. Firstly, the wind tunnel tests are always essential for a super large HCT or group of HCTs, and the tests could be conducted even if the experiment equipment is not sufficient as elaborated in the next section. Secondly, the dynamic calculation in time domain has been widely mastered which is no longer an obstacle for most wind engineers and designers. Thirdly, after obtaining the actual dynamic responses, the extreme values of internal forces or the equivalent static wind load used for structural design could be got easily as proposed by Zhang *et al.* (2017).

### 3.4 Meridian correlationship

The results of the benchmark condition have involved the true but partial correlationship along both meridian and latitude directions of the wind pressure on the tower surface. In order to obtain the perfectly correlated wind pressure in meridian direction and reserve the partial correlationship along latitude, the wind pressures got

directly from experiment were adjusted in the following procedure. If the wind pressures at a certain section (Fig. 1) at height  $z_0$  were selected as base pressures, then the pressure at other sections would be adjusted by

$$c_p(z, \theta, t) = \frac{\sigma(z, \theta)}{\sigma(z_0, \theta)} c_p(z_0, \theta, t) \quad (17)$$

in which  $c_p(z, \theta, t)$  is the fluctuating pressure history at arbitrary position  $(z, \theta)$ ;  $c_p(z_0, \theta, t)$  is the fluctuating pressure history at latitude angle  $\theta$  of the selected section;  $\sigma(z, \theta)$  and  $\sigma(z_0, \theta)$  are the rms values at position  $(z, \theta)$  and  $(z_0, \theta)$  correspondingly. In this way, the latitude correlation in any height would be the same as the selected section but perfect correlation along meridian direction would be obtained.

It should also be kept in mind that the mean pressures on the total surface as well as the mean responses still remain the same after the adjustment. Therefore, only the fluctuating responses would be altered by the pressure adjustment, and this is exactly what expected. Another, the rms values of the whole surface were also unchanged because the latitude distribution of rms values got from the wind tunnel test varies with height more or less, especially in the top and bottom regions. However, it's evident that the selection of base section would determine the final fluctuating pressures and responses because the latitude distribution of  $\sigma(z, \theta)$  and latitude correlation both vary with height (Fig. 5), so several sections in the middle shell were selected as the base section in this study, including section 2 to section 7 in Fig. 1.

Comparison of fluctuating responses got from the partial and perfect correlation along meridian direction are shown in Fig. 18. Firstly, the results of perfect correlated wind pressure in meridian direction got from different sections show quite little discrepancy especially for the total rms value of  $F_Y$ . This implies the difference of latitude rms values and correctionship of sections have little influence on the fluctuating responses. Therefore, the results of perfect correlated wind pressure got from section 5 were chose as representative for the following comparison with the benchmark condition.

The total rms value  $\sigma_T$  of  $F_Y$  increased notably when the wind pressures are adjusted from partially correlated to perfectly correlated in meridian direction, except in the top shell where  $\sigma_T$  is very small. The maximum increase is about 50% and appears in the middle shell. In the lower part, the increase is descending with height and is only 10% left at the bottom. As stated above,  $\sigma_T$  of  $F_Y$  is dominated by the background component  $\sigma_B$  and  $F_Y$  is contributed by the pressure all height, so the increase of correlation in height brings greater  $\sigma_B$  and  $\sigma_T$ . Moreover, the gust response factor  $G$  also raises when perfectly correlated pressures are employed: the  $G$  of  $F_{Y, T}$  increases from 1.48 to 1.57 at height  $h_s/H_s=0.3$  and from 1.73 to 2.12 at height  $h_s/H_s=0.7$ . According to the structural design procedure, the meridian reinforcement at height  $h_s/H_s=0.3$  and  $h_s/H_s=0.7$  increase 9% and 30% respectively, but the total meridian reinforcement increases about 11% because the requited meridian reinforcement in the top region is quite less than in the bottom region.

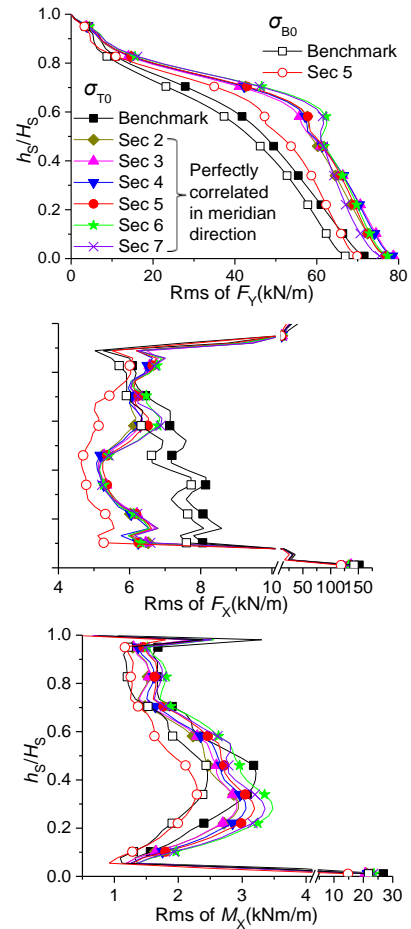


Fig. 18 Influences of meridian correlation on gust responses

For the total rms values of the two latitude internal forces, however, increase and decrease appear at different regions but the variation is not remarkable. As stated above,  $F_X$  and  $M_X$  are local internal forces, which means the correlation in meridian direction has not as much influence on  $F_X$  and  $M_X$  as on  $F_Y$ . What should be noted is that both  $\sigma_{B0}$  and  $\sigma_{T0}$  always decrease when perfectly correlated pressures are used, especially for  $F_X$  in the lower region shell. This could be also be explained by its influence function shown in Fig. 11: the higher local correlation in meridian direction, yet the lower background component for  $F_X$  because its local influence function varies above and below zero.

For structure reinforcement design, in the middle and lower regions, the decrease of  $\sigma_{T0}$  of  $F_X$  and the nearly maintaining  $\sigma_{T0}$  of  $M_X$  wouldn't reduce the latitude reinforcement in the middle and lower shell which is always determined by the minimum reinforcement requirement. In the top region, the increase of  $\sigma_T$  of  $F_X$  and the decrease of  $\sigma_T$  of  $M_X$  would approximately neutralize their influences on the latitude reinforcement. Consequently, the perfect-correlated pressure in meridian direction would just increase the meridian reinforcement to a certain and acceptable extent, but wouldn't change the latitude reinforcement amount. This is a meaningful result for the wind tunnel tests on rigid models of HCTs for wind

pressures on the whole surface: the wind pressures on the whole surface could be measured non-simultaneously.

The final application of the wind pressures is for the dynamic calculation of HCTs, which demands simultaneous measurement in high frequency on many taps distributing nearly uniformly over the tower surface and this is a great challenge for the experiment equipment. Although there is no specific requirement to comply with about the tap number and this study installed much more taps compared with other literatures, it's still not believed sufficient: the distance between certain sections is twenty eight meters if scaled to prototype and the wind pressure histories at certain locations got from POD expansion also show some discrepancy with the original wind pressure histories got directly from experiment. Of course the tap number could never catch up with the node number of the FE model and certain expansion technique is needed, but the more taps measured simultaneously, the more accurate wind pressures got through the expansion technique. However, when the equipment can only afford limited sections of taps for simultaneous measurement, all the sections could be measured non-simultaneously and converted to be simultaneous but perfectly correlated in meridian direction by virtue of Eq. (17). Taking this experiment model for example, the non-simultaneous surface pressures could be obtained by measuring three sections at a time and measuring three times in the same wind field. Then, the simultaneous wind pressure history of the whole surface could be obtained from Eq. (17). Of course the obtained wind pressures are perfectly correlated in meridian direction, but the final meridian reinforcement is conservative and acceptable.

#### 4. Conclusions

The wind induced dynamic responses are complicated functions of structure and wind properties, which could be shown clearly by the intricate expressions of gust response factors of building structures. For HCTs, the gust response factors given by different codes are much simple compared with those of building structures. The fundamental reason is there are many modes contributing to resonant effects, which is a great obstacle for the theoretical deduce of gust response factor. Another, dynamic effects of HCT shells vary greatly with responses and locations, which is also a great obstacle for the selection of equivalent target for the equivalent static wind load. So, the gust response factors given by codes or researchers are always fitted expressions obtained from limited expressions and calculation, not theoretical expressions as the building structures. Moreover, the resonant components proposed by different researcher still show notable discrepancy. In the present study, features of dynamic effects were elaborated firstly, focusing on the background and resonant components, as well as their contributions to the total rms values of different internal forces, which are the basis for the topical subject of this study. In this process, the resonant response history was separated from the total response history by a simple but accurate method. Then, the influences on the wind dynamic effects of a HCT were discussed by parameter adjustment of

four factors, the fundamental frequency, damping ratio, wind velocity and meridian correlationship.

It was shown that the resonant component is always less than the background component for all responses when only the maximum rms value along latitude is concerned, but the contributions from the resonant components still vary with responses and meridian locations. Generally speaking, the least and most contributions belong to the meridian axial force and latitude moment correspondingly, this also is part reason for the differences of gust response factors of different responses. Influence functions and the pressure correlations provide reasons for the differences of the ratios of the background component to the mean response. The resonant component for all the latitude and meridian internal forces shouldn't be neglected, and this is an overall consideration of the status of each internal force in the structural design and the contribution of the resonant component. Moreover, the coupling effects could always be ignored between the background and resonant component for all responses, even when the fundamental frequency is 0.396Hz.

The four factors impact influences on the dynamic responses in different manners. The fundament frequency is the most critical factor, and it is studied by adjusting the elastic modulus to get a series of fundament frequencies which owns unique benefits. All the resonant responses increase with the decent of the fundament frequency but with different speeds. The most sensitive response is latitude moment, followed by displacement, meridian axial force and latitude axial force. Another, a new parameter  $RP$  (Eq. (14)) is proposed to evaluate the influences from the fundament frequency. When the fundament frequency is greater than 0.7Hz, its variation shows littler influence on the gust response factors. If this is re-verified from other HCTs in further studies, 0.7Hz could also regarded as a minimal requirement for the fundament frequency of concrete HCTs. Damping ratio's influence on the resonant responses is a little simple relatively, and all the responses are influenced approximately in the same pattern which could be simply expressed by Eq. (15). The influence on the resonant component is remarkable, but the influence on the total rms value is quite limited. So, a determined damping ratio 1% could be recommended until more data are obtained from tests on prototype structures.

The influence from wind velocity is complicated. Even if the wind spectrum wouldn't change, all the components would increase with the second power of wind velocity. Actually, the wind spectrum would tend to high frequency region and bring greater resonant component. When concerning only the influence from wind spectrum variation due to velocity, the resonant component always increase linear with the velocity, which means the total resonant component would increase with the third power of wind velocity. Another, even for the common velocities in structural design, the resonant component and the total rms values of all responses would show non-negligible increase with the velocity. Considering the random combination of structural dynamic properties and the wind velocity, the rational and practical way for structural design is performing the dynamic calculation to obtain the actual dynamic responses. Of course the wind tunnel tests on the

surface pressures are required, but the pressures could be measured non-simultaneously according to the influences from the meridian correlationship and this could reduce the demand for experiment equipment. Even when perfectly correlated wind pressures in meridian direction are employed, the total rms values of most responses are still in the same level, for example the latitude internal forces, or show not much increase, for example the meridian axial force, which are conservative and acceptable for structural design.

## Acknowledgements

The authors would like to gratefully acknowledge the supports of National Science Foundation of China (51508523).

## References

- Abu-Sitta, S.H. and Hashish, M.G. (1973), "Dynamic wind stresses in hyperbolic cooling towers", *J. Struct. Div.*, **99**(9), 1823-1835.
- Armitt, J. (1973), "Vibration of cooling towers", *Paper 311 in Proceedings International Symposium Vibration Problems in Industry*, Keswick, England, April. 1-19.
- Armitt, J. (1980), "Wind loading on cooling towers", *J. Struct. Div.*, 1980, **106**(3), 623-641.
- Babu, G.R., Rajan, S.S., Harikrishna, P., Lakshmanan, N. and Arunachalam, S. (2013), "Experimental determination of wind-induced response on a model of natural draught cooling tower", *Exp. Techniques*, **37**(1), 35-46. <https://doi.org/10.1111/j.1747-1567.2011.00715.x>.
- Basu, P.K. and Gould, P.L. (1980), "Cooling towers using measured wind data", *J. Struct. Div.*, **106**(3), 579-600.
- BS 4485 Part 4. (1996), Code of Practice for Structural Design and Construction-Water Cooling Towers, British Standard Institution, London.
- Busch, D., Harte, R., and Niemann, H. J. (1998), "Study of a proposed 200m high natural draught cooling tower at power plant Frimmersdorf/Germany", *Eng. Struct.*, **20**(10), 920-927.
- Chen, K., Wei, Q.D. (2003), "Wind tunnel tests on the wind-induced vibrations", *Proceedings of the 11<sup>th</sup> National Conference on Structural Wind Engineering*, Sanya, China, 177-182.
- Davenport, A.G. and Isyumov, N. (1967), *Written Contribution of Session 3 Proc. 1<sup>st</sup> NDCT*, London, June. 97-100.
- GB/T 50102-2014. (2014), Code for design of cooling for industrial recirculating water, Ministry of Construction, P.R.C.
- Hashish, M.G. and Abu-Sitta, S.H. (1974), "Response of hyperbolic cooling towers to turbulent wind", *J. Struct. Div.*, 1974, **100**(5), 1037-1051.
- Isyumov, N., Abu-Sitta, S.H. and Davenport, A.G. (1972), "Approaches to the design of hyperbolic cooling towers against the dynamic action of wind and earthquakes", *Bull. Int. Assoc. Shell Struct.*, **48**, 35-47.
- Kapania, R.K. and Yang, T.Y. (1984), "Time domain random wind response of cooling tower", *J. Eng. Mech.*, **110**(10), 1524-1543. [https://doi.org/10.1061/\(ASCE\)0733-9399\(1984\)110:10\(1524\)](https://doi.org/10.1061/(ASCE)0733-9399(1984)110:10(1524)).
- Kasperski, M. and Niemann, H.J. (1988) "On the correlation of dynamic wind loads and structural response of natural-draught cooling towers", *J. Wind Eng. Ind. Aerod.*, **30**(1-3), 67-75. [https://doi.org/10.1016/0167-6105\(88\)90072-4](https://doi.org/10.1016/0167-6105(88)90072-4).
- Ke, S.T., Ge, Y.J., Zhao, L. and Tamura, Y. (2012), "A new methodology for analysis of equivalent static wind loads on super-large cooling towers", *J. Wind Eng. Ind. Aerod.*, **111**, 30-39. <https://doi.org/10.1016/j.jweia.2012.08.001>.
- Ke, S.T., Ge, Y.J. and Zhao, L. (2015), "Wind-induced vibration characteristics and parametric analysis of large hyperbolic cooling towers with different feature sizes", *Struct. Eng. Mech.*, **54**(5), 891-908. <https://doi.org/10.12989/sem.2015.54.5.891>.
- Ke, S.T., Wang, H. and Ge, Y.J. (2018a), "Multi-dimensional extreme aerodynamic load calculation in super-large cooling towers under typical four-tower arrangements", *Wind Struct.*, **25**(2), 101-129. <https://doi.org/10.12989/was.2017.25.2.101>.
- Ke, S.T., Du, L.Y., Ge, Y.J. and Tamura, Y. (2018b), "Multi-dimensional wind vibration coefficients under suction for ultra-large cooling towers considering ventilation rates of louvers", *Struct. Eng. Mech.*, **66**(2), 273-283. <https://doi.org/10.12989/sem.2018.66.2.273>.
- Ke, S.T., Yu, W., Xu, L., Ge, Y.J. and Tamura, Y. (2018c), "Identification of damping ratio and its influences on wind- and earthquake-induced effects for large cooling towers", *Struct. Des. Tall Spec.*, **27**(12), 1-20. <https://doi.org/10.1002/tal.1488>.
- Lu, W.D., Wang, Y.Q., Peng, J.X. and Lin, B.Q. (1982), "Response of hyperbolic cooling tower to turbulent wind", *Pro. CSEE*, (1), 45-61.
- Niemann, H.J. (1980), "Wind effects on cooling-tower shells", *J. Struct. Div., ASCE*, 1980, **106**(3), 643-661.
- Niemann, H.J. (1984), "Modelling of wind loads with regard to gust effects", *Eng. Struct.*, **6**(4), 274-280. [https://doi.org/10.1016/0141-0296\(84\)90024-5](https://doi.org/10.1016/0141-0296(84)90024-5).
- Niemann, H.J. and Ruhwedel, J. (1980), "Full-scale and model tests on wind-induced, static and dynamic stresses in cooling tower shells", *Eng. Struct.*, **2**(2), 81-89. [https://doi.org/10.1016/0141-0296\(80\)90034-6](https://doi.org/10.1016/0141-0296(80)90034-6).
- Noh, S.Y. and Lee, S.Y. (2012), "Evaluation of the natural draught cooling tower shell using linearly and non-linearly numerical analysis", *J. Vibroeng.*, **14**(3), 1011-1020.
- Singh, M.P. and Gupta, A.K. (1976), "Gust factors for hyperbolic cooling towers", *J. Struct. Div.*, **102**(2), 371-386.
- Sollenberger, N.J., Scanlan, R.H. and Billington, D.P. (1980), "Wind loading and response of cooling towers", *J. Struct. Div., ASCE*, **106**(3), 601-621.
- Steinmetz, R.L., Abel, J.F. and Billington, D.P. (1978), "Hyperbolic cooling tower dynamic response to wind", *J. Struct. Div., ASCE*, **104**(1), 35-53.
- VGB-R 610Ue (2005), VGB-Guideline: Structural design of cooling tower-technical guideline for the structural design, computation and execution of cooling towers, BTR Bautechnik bei Kühltürmen, Essen.
- Zhang, J.F., Ge, Y.J. and Zhao, L. (2013) "Influence of latitude wind pressure distribution on the responses of hyperboloidal cooling tower shell", *Wind Struct.*, **16**(6), 579-601.
- Zhang, J.F., Ge, Y.J., Zhao, L. and Ke, S.T. (2013), "Wind tunnel study on the three dimensional flow and spatial correlation properties of wind loads on hyperboloidal cooling towers", *Eng. Mech.*, **30**(9), 234-242.
- Zhang, J.F., Ge, Y.J., Zhao, L., and Zhu, B. (2017), "Wind induced dynamic responses on hyperbolic cooling tower shells and the equivalent static wind load", *J. Wind Eng. Ind. Aerod.*, **169**, 280-289. <https://doi.org/10.1016/j.jweia.2017.08.002>.
- Zhao, L., Chen, X., Ke, S.T. and Ge, Y.J. (2014), "Aerodynamic and aero-elastic performances of super-large cooling towers", *Wind Struct.*, **19**(4), 443-465. <https://doi.org/10.12989/was.2014.19.4.443>.
- Zhao, L., Ge, Y.J. and Cao, F.C. (2008), "Equivalent beam-net design theory of aero-elastic model about hyperbolic thin-shell cooling towers and its experimental investigation", *J. Vibra. Eng.*, **21**(1), 31-37.
- Zhao, L., Zhan, Y.Y. and Ge, Y.J. (2018), "Wind-induced equivalent static interference criteria and its effects on cooling towers with complex arrangements", *Eng. Struct.*, **172**, 141-153.

<https://doi.org/10.1016/j.engstruct.2018.05.117>.

Zou, Y.F., Niu, H.W., Chen, Z.Q. (2013), "Wind tunnel test on wind-induced response of cooling tower based on full aero-elastic model", *J. Build. Struct.*, **34**(6), 60-67.

CC